



ANALYSES OF WRINKLING AND BUCKLING OF ELASTIC PLATES BY DXDR METHOD

M. Kadkhodayan†, L. C. Zhang†§ and R. Sowerby‡

†Centre for Advanced Materials Technology, Department of Mechanical and Mechatronic Engineering, The University of Sydney, NSW 2006, Australia

‡Department of Mechanical Engineering, McMaster University, Hamilton, Ontario, Canada L8S 4L7

(Received 26 April 1995)

Abstract—This paper deals with the wrinkling and buckling of elastic plates subjected to in-plane and transverse external forces. With the aid of a newly developed dynamic relaxation method, the well-known dynamic criterion of stability was used to predict the bifurcation point. Some typical components in engineering practice (i.e. annular, circular and rectangular plates) were investigated in detail. The reliability of the method for the analyses of post-wrinkling and post-buckling was demonstrated. Based on the analytical studies performed, approximate formulas for determining the critical load and number of waves in the wrinkling mode were obtained. It found that the initial elastic wrinkling mode of plates subjected to bending was different from that of plastic wrinkling. © 1997 Elsevier Science Ltd.

NOTATION

a	length of a rectangular plate
b	width of the rectangular plate
C	diagonal damping matrix ($[c_{ij}]$)
D	flexural rigidity of a plate, $Eh^3/12(1 - \nu^2)$
E	Young's modulus
F	vector of generalised forces of a discrete system
G	shear modulus
h	thickness of a plate
K	stiffness matrix of the discrete system
k	qR_0^2/D
k^*	$qb^2/\pi^2 D$
M	diagonal mass matrix of the discrete system ($[m_i^*]$)
M	bending or twisting moment
m	number of waves of a wrinkling mode
N	membrane force
N_{total}	total node number of the discrete system
P	vector of internal forces of the discrete system
q	uniformly distributed in-plane load
R	vector of residual forces of the discrete system
R	radius of a circular plate
R_i	inner radius of the annular plate
R_o	outer radius of the annular plate
u, v, w	displacement components in x, y and z directions, respectively
X	vector of generalised solution of the discrete system
\dot{X}, \ddot{X}	vectors of fictitious velocity and acceleration of the discrete system, respectively
z	direction normal to the mid-plane of the plate

Greek letters

β	R_i/R_o
γ	shear strain
$\delta(\dots)$	a small increment of quantity (...)
ϵ	normal strain
ζ	critical node damping factor
κ	curvature of the plate

ξ	$1 - \beta$
σ	normal stress
τ	increment of fictitious time
τ_{xy}	shear stress component
ν	Poisson's ratio

Superscripts and subscripts

i	node i
L	indication of three perpendicular coincident with displacement u, v and w , respectively
n	the n th iteration step
x, y	x and y directions, respectively
r, θ	r and θ directions, respectively

1. INTRODUCTION

Wrinkling and buckling are the common failure modes of many plate and shell structures in engineering. The prediction or detection of the onset of wrinkling and buckling and the reliable analyses of post-wrinkling and post-buckling have long been the important topics of research for engineers and scientists. It is understood that the onset of wrinkling/buckling is the bifurcation point on the loading path of a structure from the primary equilibrium path to the secondary equilibrium path. Correspondingly, there are three equivalent criteria for predicting the bifurcation of conservative systems: static, energy and dynamic criteria. However, the former two criteria are not valid for non-conservative problems and the application of the dynamic criterion is difficult. Hence, the development of an appropriate algorithm for bifurcation prediction when using the dynamic criterion is of practical importance.

§ Author to whom correspondence should be addressed.

Based on their newly developed numerical method of modified adaptive dynamic relaxation (maDR), Zhang *et al.* [1] and Zhang and Yu [2], embodied the dynamic criterion of stability within their algorithm, and investigated the plastic wrinkling of circular plates stamped by rigid punches. Their approach successfully overcomes the difficulties of applying this important stability criterion to engineering problems. However, because of the lower convergence rate of the DR type method, the computational time for performing a wrinkling analysis is still considerable.

The purpose of this paper is two-fold. The first is to combine a more powerful dynamic relaxation method developed by Zhang and his co-workers [10] with the dynamic criterion to offer a more efficient analysis of wrinkling/buckling and post-wrinkling/buckling. The second is to gain more knowledge of wrinkling and buckling through the detailed analysis of some typical engineering components by this unique approach.

2. DETECTION OF BIFURCATION POINT

As pointed out by Zhang *et al.* [1], the main difficulties in the application of the dynamic criterion of stability are that a static mechanics system must be treated as a dynamic one (an initial value problem) and that the stability of the system must be monitored until time t approaches to infinity when the system is subjected to any kind of initial disturbances. Fortunately, these difficulties can be overcome naturally when the dynamic relaxation method is used [1-2]. This type of method searches for static solutions of an equilibrium system by making use of the dynamic transient analysis (see the appendix and Refs [1-2] for details). The initial dynamic distur-

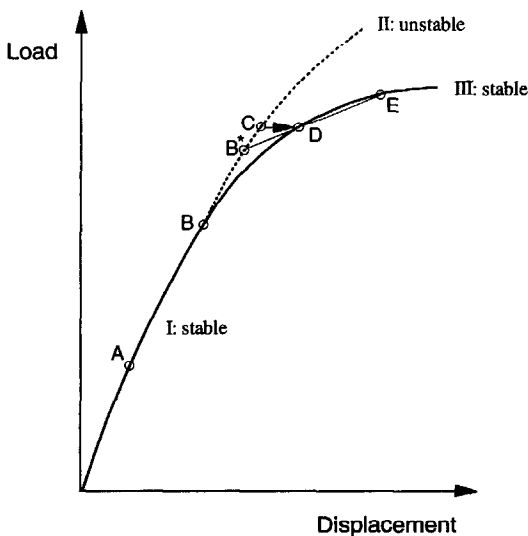


Fig. 1. Bifurcation of equilibrium state of a mechanical system.

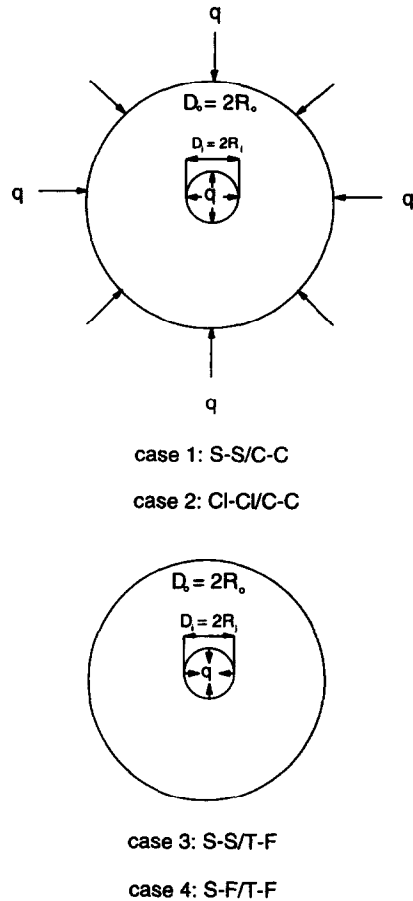
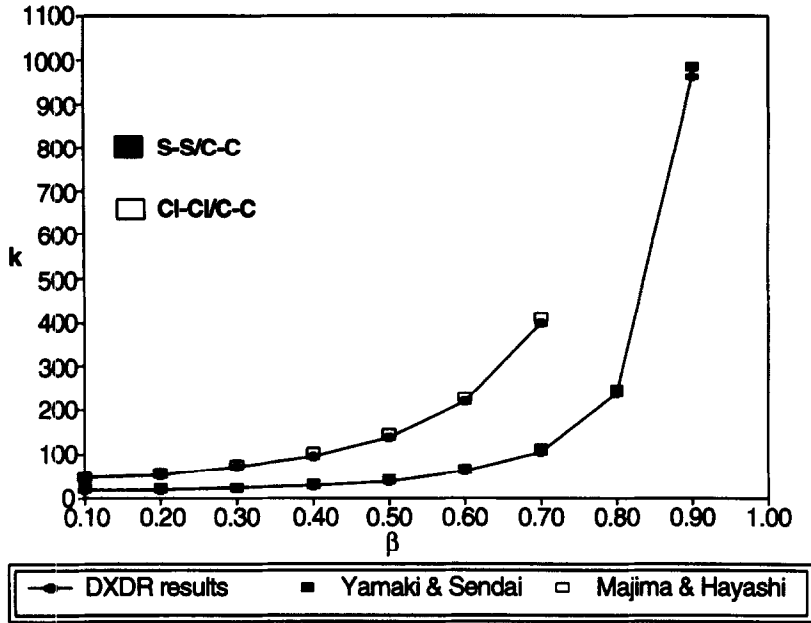


Fig. 2. Loading and boundary conditions of annular plates: (a) S-S/C-C and Cl-Cl/C-C; (b) S-S/T-F and S-F/T-F.

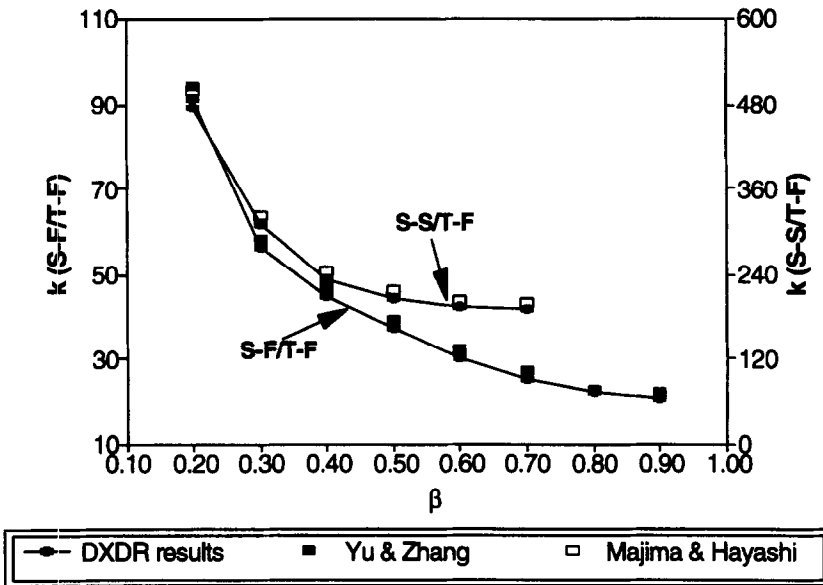
ances generated by the disequilibrium internal forces are arbitrary and the iteration for obtaining the correct static solution is with respect to time. Therefore, the stability of the system can be observed in a practical time interval.

Figure 1 shows the method of determining the bifurcation point by the dynamic relaxation method, where curve I is the primary equilibrium path of a mechanics system, curve III the secondary equilibrium path after bifurcation and curve II is an unstable equilibrium path. When the state of the system is on curve I, say at point A, the fictitious vibration of the dynamic relaxation is stable. However, if the deformation state of the system goes beyond the bifurcation point B (e.g. at point C), the vibration becomes unstable, and a jump from C to D occurs, and then a stable vibration around state point D starts. Once two points like D are detected, an approximate bifurcation point B* can be obtained by a linear extrapolation. Further deformation of the system moves the corresponding state along curve III, which represents the post-wrinkling/buckling states of the system.

To perform the bifurcation prediction illustrated above, one can use different methods or algorithms



(a)



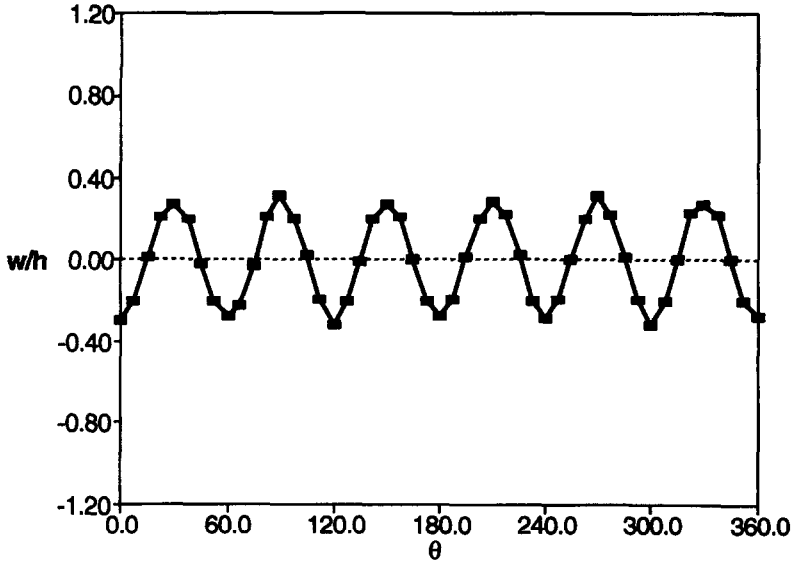
(b)

Fig. 3. Wrinkling load parameters: (a) for S-S/C-C and Cl-CI/C-C; (b) for S-S/T-F and S-F/T-F.

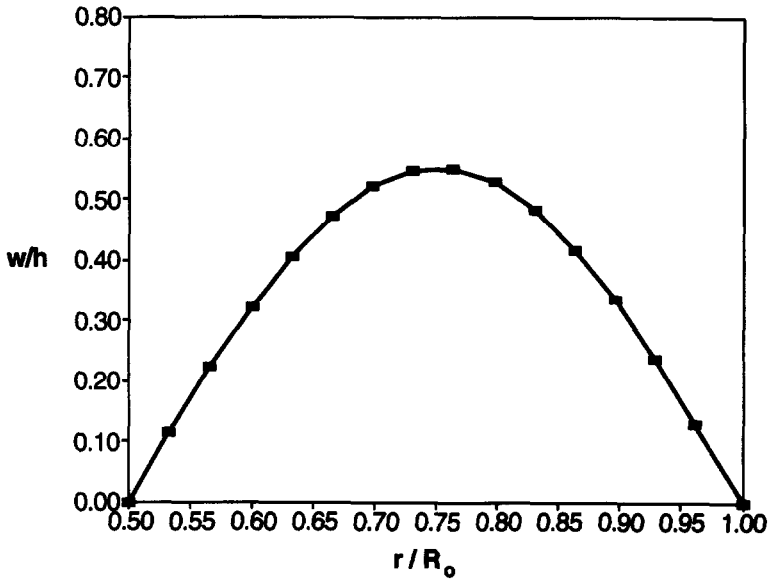
depending on the problem under review. The following proposed method is extremely suitable for the problems to be analysed in this paper. In its pre-wrinkling/buckling states (states on the primary equilibrium path), the slope of deflection at any point in a plate is zero†. If a non-zero slope is detected at a certain load level, it corresponds to a

post-wrinkling/buckling state on the secondary equilibrium path III. If two such points are obtained, say D and E in Fig. 1, the approximate bifurcation point B^* from path I to III can be determined simply by an extrapolation from these two points. The accuracy of B^* obtained, compared with the real bifurcation point B, depends on the relative state distance of D and E from B. To get a sufficiently accurate prediction, an iteration is usually needed to find better post-wrinkling/buckling state points closer to B.

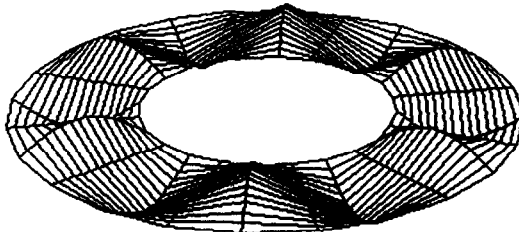
† For a circular plate under axisymmetric transverse bending, the circumferential deflection slope at any point in the pre-wrinkling state is always zero.



(a)

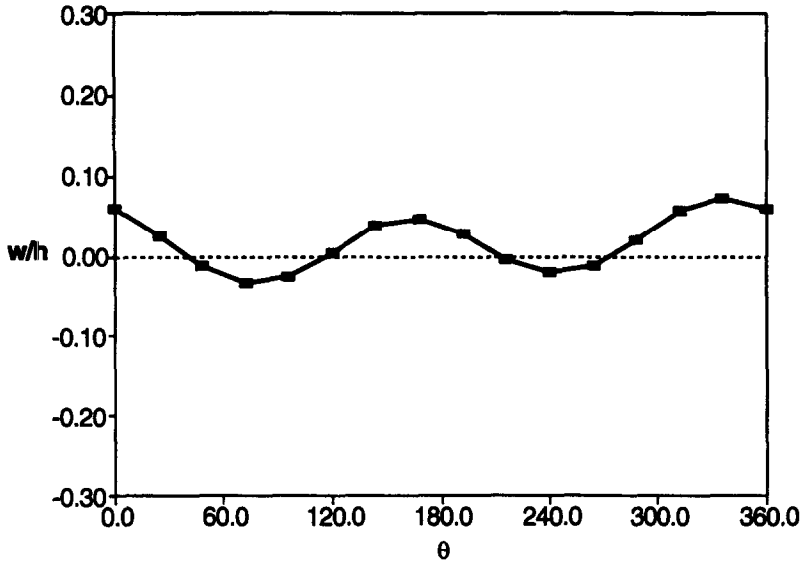


(b)

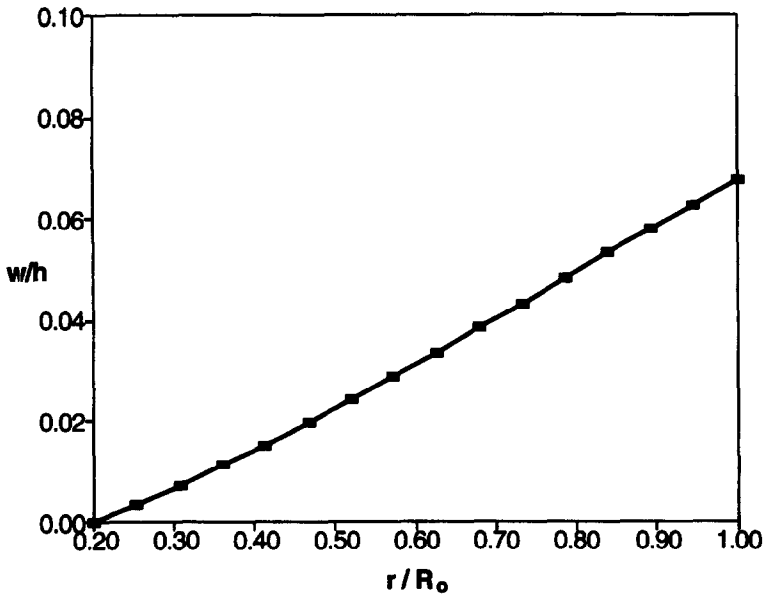


(c)

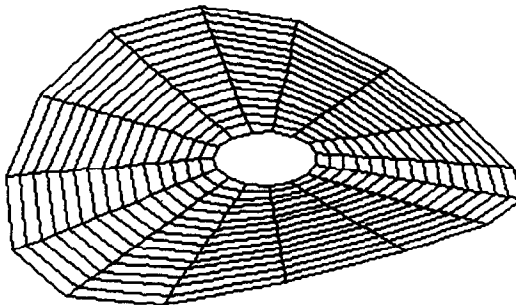
Fig. 4. Wrinkling mode of S-S/T-F as $\beta = 0.5$: (a) in $z-\theta$ plane at $r = (R_1 + R_0)/2$; (b) in $z-r$ plane; (c) in 3-D form.



(a)



(b)



(c)

Fig. 5. Wrinkling mode of S-F/T-F as $\beta = 0.2$: (a) in $z-\theta$ plane at $r = R_0$; (b) in $z-r$ plane; (c) in 3-D form.

Table 1. Number of waves in different annular plates

ξ	0.3	0.4	0.5	0.6	0.7	0.8
$m(\text{case 1})$	0	0	0	0	0	0
$m(\text{case 2})$	7	5	4	3	2	2
$m(\text{case 3})$	9	7	6	5	4	3
$m(\text{case 4})$	4	3	3	2	2	2

3. CASE STUDIES AND DISCUSSION

Three problems have been analysed herein to assess the method outlined in the preceding section. These are the elastic wrinkling/buckling of an annular plate subjected to an in-plane load, a circular plate under transverse ring load and a rectangular plate compressed by in-plane loads. The wrinkling/buckling of annular plates under various loading conditions has been investigated by many researchers. Yamaki and Sendai [3] studied the buckling of a thin annular plate under uniform compressive edge forces using an analytical method. Majima and Hayashi [4] analysed an annular plate subjected to a non-uniform in-plane stress by the Galerkin method. Yu and Johnson [5] studied the problem in relation to the deep-drawing process by means of the energy method. Yu and Zhang [6] investigated the elastic wrinkling of an annular plate using a hybrid approach which combined the Kantorovich and Galerkin methods. A common characteristic of all these studies is that either a static or energy criterion was used for predicting the bifurcation. The wrinkling of a circular plate subjected to a transverse ring load has been analysed by Zhang *et al.* [1]. However, in seeking for a bifurcation point, they monitored the incremental displacement in the circumferential direction that is more difficult and less efficient compared with the method proposed in the last section. Yu and Stronge analysed the wrinkling of a circular elastic plate stamped by a spherical punch by energy method [7]. Although the wrinkling/buckling behavior of annular and rectangular plates have received considerable attention, a further analysis of the problem does serve a useful purpose. The results that have been gathered to date provides a useful yardstick against which to judge the applicability and reliability of the proposed algorithm for bifurcation analysis. In all the calculations below, the materials constants used are Young's modulus $E = 206$ GPa and Poisson's ratio $\nu = 0.3$.

Table 2. Parameters to calculate the number of waves

	Δ	Λ
case 1	—	—
case 2	2.39	0.96
case 3	2.77	0.03
case 4	0.45	1.72

3.1. Elastic wrinkling of annular plates

Both loading and boundary conditions can alter the deformation mechanisms of an annular plate. Therefore, to investigate the effects of these factors, the following four cases are studied:

Case 1. Both the inner and outer edges are simply supported and subjected to in-plane uniform compressive forces, S-S/C-C, Fig. 2(a).

Case 2. Both edges are clamped and subjected to in-plane uniform compressive forces, C1-C1/C-C, Fig. 2(a).

Case 3. Both edges are simply supported. The plate is subjected to in-plane tensile force on its inner edge, but its outer edge is traction free, S-S/T-F, Fig. 2(b).

Case 4. The inner edge is simply supported and the outer edge is free. The plate is under an in-plane tensile force on its inner edge only, S-F/T-F, Fig. 2(b).

The incremental form of the equilibrium equations for an annular plate are

$$\begin{aligned}
 \frac{\partial \delta N_r}{\partial r} + \frac{1}{r} \frac{\partial \delta N_{r\theta}}{\partial \theta} + (\delta N_r - \delta N_\theta) &= 0, \\
 \frac{\partial \delta N_{r\theta}}{\partial r} + \frac{1}{r} \frac{\partial \delta N_\theta}{\partial \theta} + \frac{2}{r} (\delta N_{r\theta}) &= 0, \\
 \frac{\partial^2 \delta M_r}{\partial r^2} + \frac{1}{r} \left(2 \frac{\partial \delta M_r}{\partial r} - \frac{\partial \delta M_\theta}{\partial r} \right) + \frac{2}{r} \frac{\partial^2 \delta M_{r\theta}}{\partial r \partial \theta} \\
 + \frac{2}{r^2} \frac{\partial \delta M_{r\theta}}{\partial \theta} + \frac{1}{r^2} \frac{\partial^2 \delta M_\theta}{\partial \theta^2} + (N_r + \delta N_r) \frac{\partial^2 \delta w}{\partial r^2} \\
 + \delta N_r \frac{\partial^2 w}{\partial r^2} + \frac{2}{r} \left[\frac{\partial^2 \delta w}{\partial r \partial \theta} (N_{r\theta} + \delta N_{r\theta}) \right. \\
 \left. + \frac{\partial^2 w}{\partial r \partial \theta} \delta N_{r\theta} \right] - \frac{2}{r^2} \left[\frac{\partial \delta w}{\partial \theta} (N_\theta + \delta N_\theta) \right. \\
 \left. + \frac{\partial w}{\partial \theta} \delta N_\theta \right] + \left(\frac{1}{r} \frac{\partial w}{\partial r} + \frac{1}{r^2} \frac{\partial^2 w}{\partial \theta^2} \right) \delta N_\theta \\
 + \left(\frac{1}{r} \frac{\partial \delta w}{\partial r} + \frac{1}{r^2} \frac{\partial^2 \delta w}{\partial \theta^2} \right) (N_\theta + \delta N_\theta) &= 0, \quad (1)
 \end{aligned}$$

Table 3. Coefficients to determine the critical loads

	α_1	α_2	α_3	α_4	α_5
case 1	71.2	-83.9	47.6	-8.2	4.6
case 2	144.7	-411.2	451.8	-240.0	61.5
case 3	105,875.0	-178,855.0	11,1045.0	-30,472.7	3423.3
case 4	1439.4	-3635.4	3394.8	-1439.3	273.4

where

$$(\delta N_r, \delta N_\theta, \delta N_{r\theta}, \delta M_r, \delta M_\theta, \delta M_{r\theta}) = \int_{-h/2}^{h/2} (\delta \sigma_r, \delta \sigma_\theta, \delta \tau_{r\theta}, z \delta \sigma_r, z \delta \sigma_\theta, z \delta \tau_{r\theta}) dz, \quad (2)$$

are the incremental membrane forces, bending and twisting moments, respectively. The geometrical relations between the incremental strains and displacements are

$$\begin{aligned} \delta \epsilon_r &= \delta \epsilon_r^0 + z \delta \kappa_r, \\ \delta \epsilon_\theta &= \delta \epsilon_\theta^0 + z \delta \kappa_\theta, \\ \delta \gamma_{r\theta} &= \delta \gamma_{r\theta}^0 + z \delta \kappa_{r\theta}, \end{aligned} \quad (3)$$

where

$$\begin{aligned} \delta \epsilon_r^0 &= \frac{\partial \delta u}{\partial r} + \frac{\partial w}{\partial r} \frac{\partial \delta w}{\partial r} + \frac{1}{2} \left(\frac{\partial \delta w}{\partial r} \right)^2, \\ \delta \epsilon_\theta^0 &= \frac{\partial u}{r} + \frac{1}{r} \frac{\partial \delta v}{\partial \theta} \\ &\quad + \frac{1}{r^2} \frac{\partial w}{\partial \theta} \frac{\partial \delta w}{\partial \theta} + \frac{1}{2} \left(\frac{1}{r} \frac{\partial \delta w}{\partial \theta} \right)^2, \\ \delta \gamma_{r\theta}^0 &= \frac{1}{r} \frac{\partial \delta u}{\partial \theta} + \frac{\partial \delta v}{\partial r} - \frac{\delta v}{r} + \frac{1}{r} \frac{\partial \delta w}{\partial r} \\ &= \times \left(\frac{\partial w}{\partial \theta} + \frac{\partial \delta w}{\partial \theta} \right) + \frac{\partial w}{\partial r} \left(\frac{1}{r} \frac{\partial \delta w}{\partial \theta} \right), \end{aligned} \quad (4)$$

$$\delta \kappa_r = -\frac{\partial^2 \delta w}{\partial r^2},$$

$$\delta \kappa_\theta = -\left(\frac{1}{r} \frac{\partial \delta w}{\partial r} + \frac{1}{r^2} \frac{\partial^2 \delta w}{\partial \theta^2} \right),$$

$$\delta \kappa_{r\theta} = -\frac{1}{r} \frac{\partial^2 \delta w}{\partial r \partial \theta} + \frac{1}{r^2} \frac{\partial_{r\theta} w}{\partial \theta}.$$

The results obtained are shown in Fig. 3 and compared with those of Yamaki and Sendai [3], Majima and Hayashi [4]† and Yu and Zhang [6]. They are in very good agreement. This demonstrates once again that the dynamic, energy and static criteria are equivalent for conservative problems.

The variation of the wrinkling load parameter with the ratio of inner radius to outer radius of the plate, β , for cases 1 and 2 are demonstrated in Fig. 3(a). The required load to initiate wrinkling for case 1 is less than that for case 2, as expected. For both cases, the wrinkling load parameter, k , increases with increasing ratio β ($R_0 = \text{constant}$). In other words, the wrinkle resistance of an annular plate with larger blank width is higher.

Figure 3(b) presents the results of the annular plates of cases 3 and 4. The required load to initiate the wrinkling of S-S/T-F is much higher compared with S-F/T-F. By contrast to cases 1 and 2, the wrinkling load parameter k of these two cases decreases as β increases, indicating that the wrinkle resistance of an annular plate with larger blank width is lower. Clearly, boundary and loading conditions alter the stress distribution in the plates and thus the wrinkling behaviour.

The wrinkling modes for cases 3 ($\beta = 0.5$) and 4 ($\beta = 0.2$) are shown in Figs 4 and 5. Table 1 lists the number of waves, m , of all cases studied when $\xi = 1 - \beta$ varies. Based on these, empirical formulas for determining the critical load and the number of waves of the wrinkling mode can be obtained, which may prove to be of practical worth. It is obvious that when ξ increases, i.e. when the width of the plate increases, the number of waves decrease. Therefore, the relationship between m and ξ can be expressed by

$$m = \frac{\Delta}{\xi} + A, \quad (5)$$

where Δ and A are constants (see Table 2) that best fitted the results in Table 1. The critical wrinkling loads of different cases have different variation trends when loading and boundary conditions differ. However, a fourth-order polynomial of β can properly describe the variation and provide an empirical prediction. If the wrinkling load parameter k is expressed as

$$k = \alpha_1 \beta^4 + \alpha_2 \beta^3 + \alpha_3 \beta^2 + \alpha_4 \beta + \alpha_5, \quad (6)$$

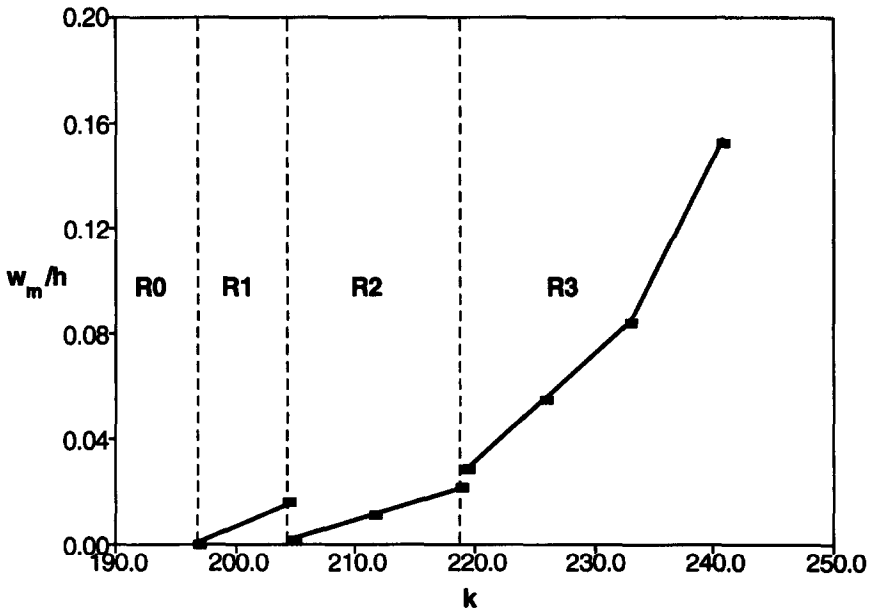
† To compare the present results to those of Majima and Hayashi [4], the wrinkling load parameter was changed from qR^2D to qR_0^2D .

the coefficients $\alpha_i (i = 1, \dots, 5)$ can be calculated easily, as listed in Table 3.

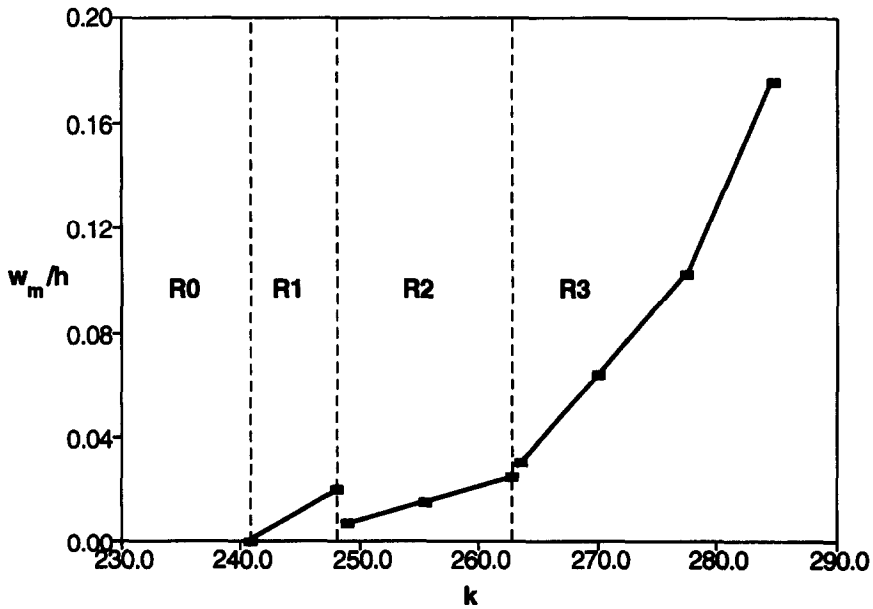
Figure 5(b) shows the radial profile of the plate S-F/T-F (case 4) in the post-wrinkling stage. The radial wrinkling mode of the plate is a nonlinear function of r . This is consistent with the solution based on a hybrid approach of the Kantorovich and Galerkin methods [7]. It has been found that the

non-linear profile of the radial mode has a significant effect on the critical load prediction when using an analytical method, though its non-linearity is not strong [6].

Now let us look at the wrinkle development of the annular plates in their post-wrinkling stages. The feature of the wrinkle growth for S-S/T-F is demonstrated in Fig. 6 with $\beta = 0.4$ and 0.6 , where



(a)



(b)

Fig. 6. Wrinkle growth in S-S/T-F: (a) $\beta = 0.4$; (b) $\beta = 0.6$.

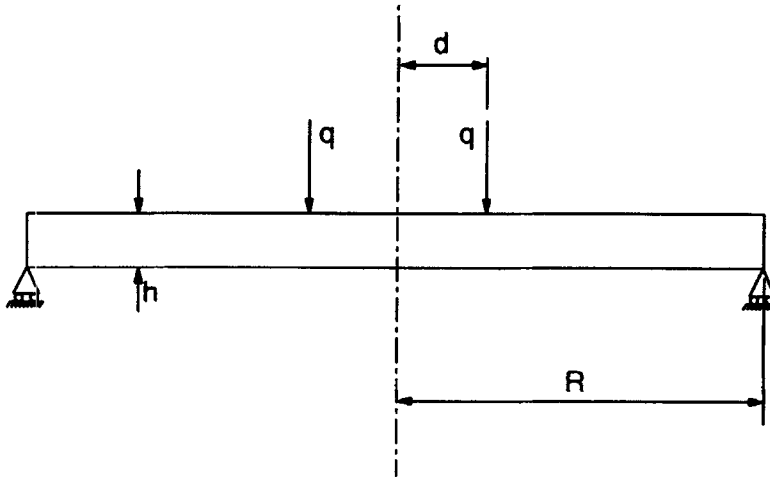


Fig. 7. A simply-supported circular plate subjected to a ring load.

w_m is the average absolute value of the wrinkle heights. For convenience, we indicate in Fig. 6 the pre-wrinkling stages as R0, the first post-wrinkling stage R1 and so on. When a plate is first wrinkled, it enters the deformation stage R1. With increasing the external load, a sudden change of wrinkling mode occurs when the load reaches to a certain value and the plate deformation is in its second post-wrinkling stage R2. We may call this load the secondary critical load. In other words, the first post-wrinkling stage becomes unstable when the secondary critical load is reached. Thus a new bifurcation takes place. Similarly, there exists a third critical load between the post-wrinkling stages R2 and R3. A further increment of the external load may bring about the fourth post-wrinkling stage and so forth. For the present annular plate, the number of waves for $\beta = 0.4$ and 0.6 in stages R1, R2 and R3 is,

respectively, $(m_1, m_2, m_3) = (5, 6, 4)$ and $(7, 8, 6)$. When the wrinkling changes from R1 to R2 w_m decreases, but when it happens from R2 to R3 w_m increases. This could be interpreted by the constant deformation energy at a critical load. The number of waves of the wrinkling mode in R2 is more than that in R1 ($5 \rightarrow 6$ when $\beta = 0.4$ and $7 \rightarrow 8$ when $\beta = 0.6$), but the deformation energy in the plate is a constant at the critical load. Hence, w_m must reduce from R1 to R2. Similarly, w_m must increase from R2 to R3 because m_3 is less than m_2 .

3.2. Elastic wrinkling of a circular plate subjected to a ring load

Wrinkling can also occur in plates subjected to transverse bending. Consider a simply supported circular plate with a movable periphery subjected to a transverse ring load, q , Fig. 7. The edge of the plate

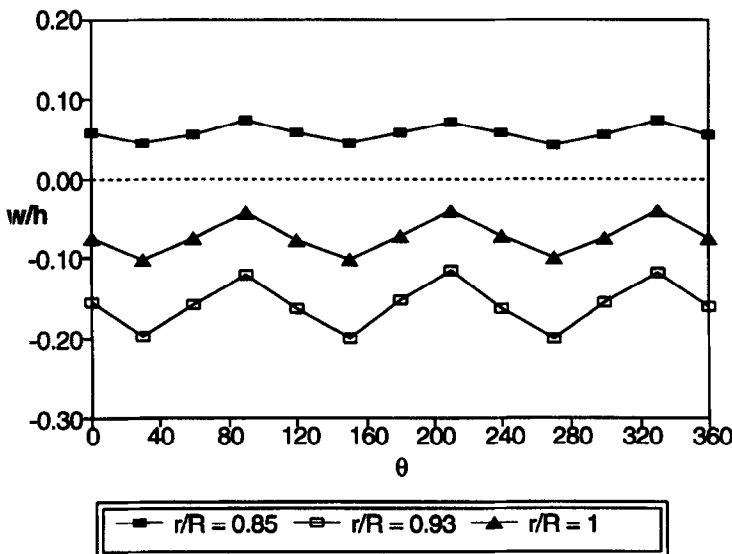


Fig. 8. The circumferential wrinkling mode at different radii of the circular plate.

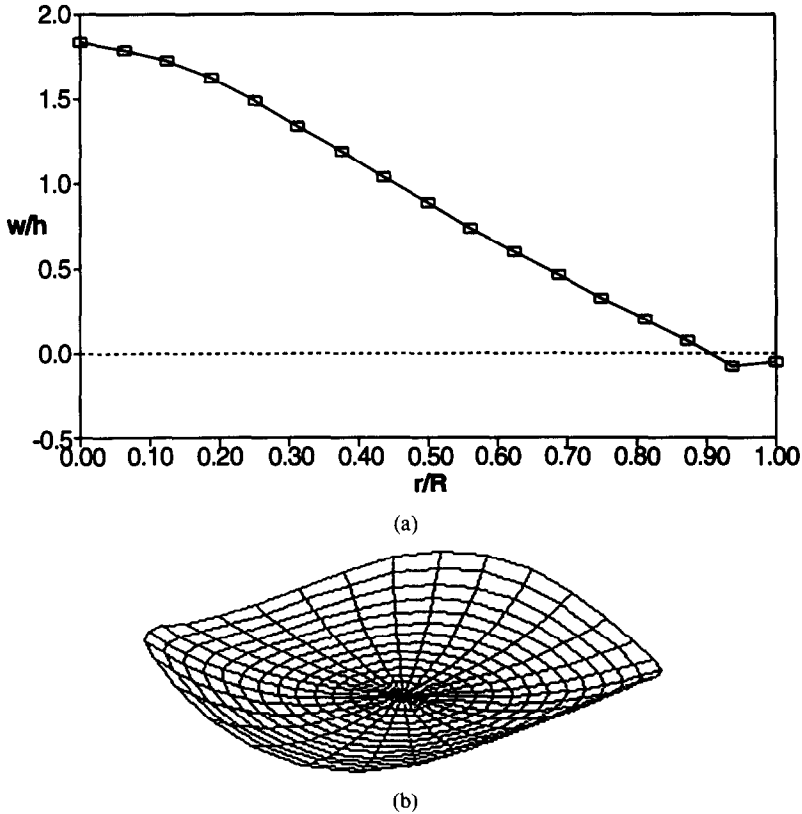


Fig. 9. The wrinkling mode of the circular plate: (a) in $z-r$ plane; (b) in 3-D form.

is free to move upward from the support. The plate is of radius $R = 75$ mm and thickness $h = 1$ mm. The radius of the ring load is $R_r = 32.5$ mm. The incremental equations for wrinkling analysis is same as the annular plate, eqns (1)–(4), provided that a term δq be added to the right hand side of eqn (1c). In the first stage the bending of the

plate is axisymmetrical, but the circumferential compressive stress near the plate periphery increases as the deflection proceeds. When this stress becomes sufficiently large, the equilibrium configuration of the plate changes from its axisymmetric state to nonaxisymmetric one. Wrinkling therefore occurs.

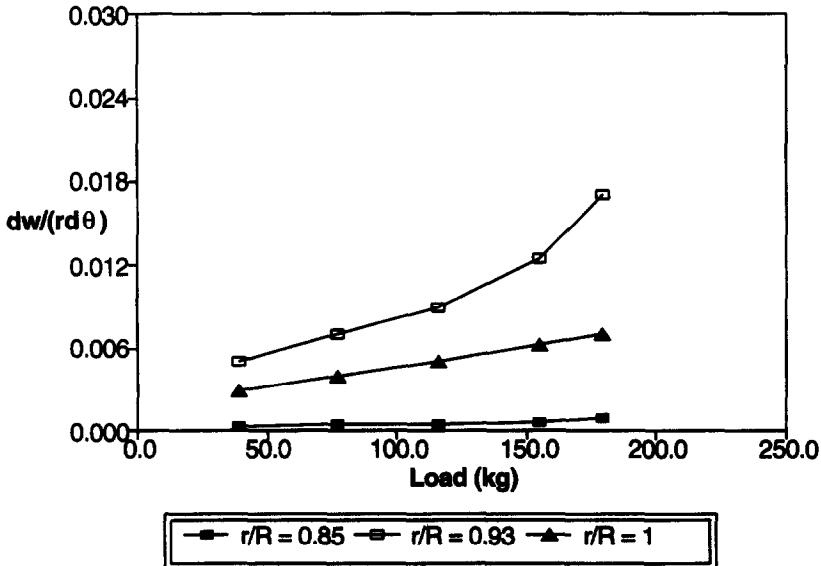


Fig. 10. The circumferential slope-load curve at different radii.

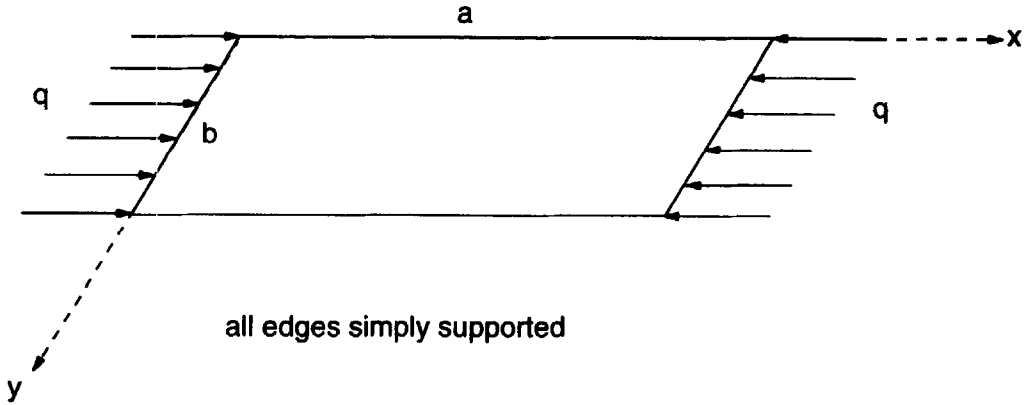


Fig. 11. A simply-supported rectangular plate under uni-axial compressive loads.

Figure 8 shows the circumferential wrinkling mode of the plate at different radii from the plate centre. It is obvious that the initial elastic wrinkling mode is with three circumferential waves which is different from that of plastic wrinkling [1]. When wrinkling appears, parts of the plate near the edge move upwards and generate negative deflections, Fig. 9(a). Figure 9(b) illustrates the three-dimensional profile of the plate after wrinkling. The variation of $1/r(\delta w/\delta \theta)$ at three different radial distances, r/R , is shown in the Fig. 10 which indicates that the radial peak of the wrinkling wave does not occur at the periphery of the plate, but at some point inside it, which is consistent with experimental observations [1, 7, 8].

3.3. Elastic wrinkling of a rectangular plate

It is assumed that the rectangular plate is simply-supported and is subjected to a uniform compressive force in x -direction, Fig. 11. The

incremental form of the equilibrium equations for the rectangular plate are

$$\begin{aligned} \frac{\partial \delta N_x}{\partial x} + \frac{\partial \delta N_{xy}}{\partial y} &= 0, \\ \frac{\partial \delta N_y}{\partial y} + \frac{\partial \delta N_{xy}}{\partial x} &= 0, \\ \frac{\partial^2 \delta M_x}{\partial x^2} + \frac{\partial^2 \delta M_y}{\partial y^2} - 2 \frac{\partial^2 \delta M_{xy}}{\partial x \partial y} &+ \delta N_x \frac{\partial^2 w}{\partial x^2} + (N_x + \delta N_x) \frac{\partial^2 w}{\partial x^2} + \delta N_y \frac{\partial^2 w}{\partial y^2} \\ &+ (N_y + \delta N_y) \frac{\partial^2 w}{\partial y^2} + 2 \delta N_{xy} \frac{\partial^2 w}{\partial x \partial y} \\ &+ 2(N_{xy} + \delta N_{xy}) \frac{\partial^2 w}{\partial x \partial y} = 0, \end{aligned} \tag{7}$$

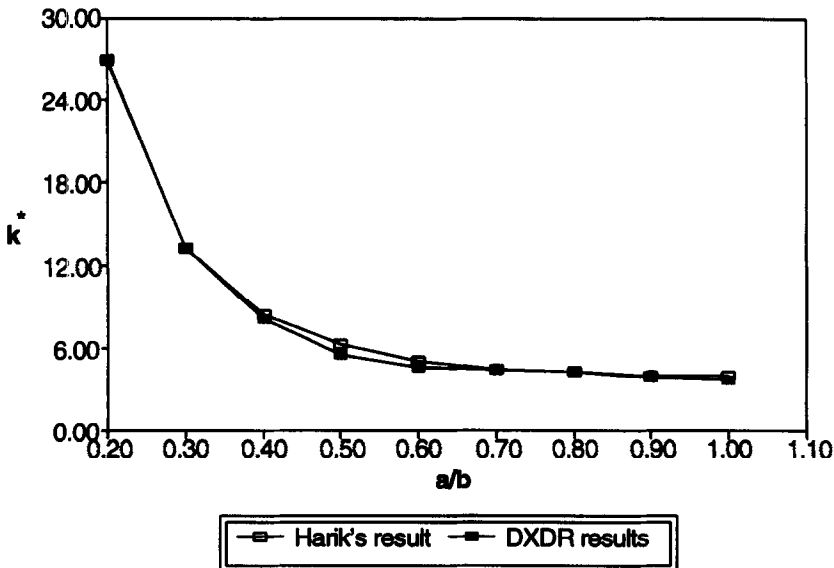
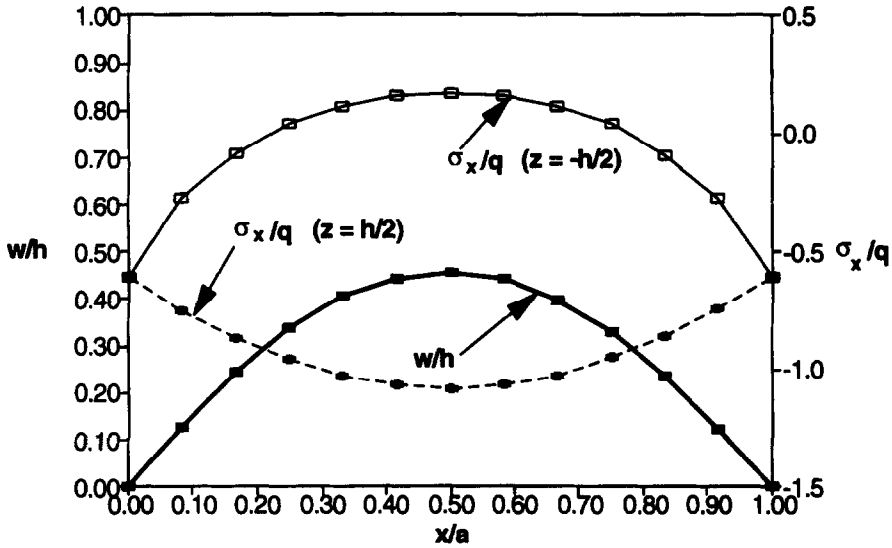
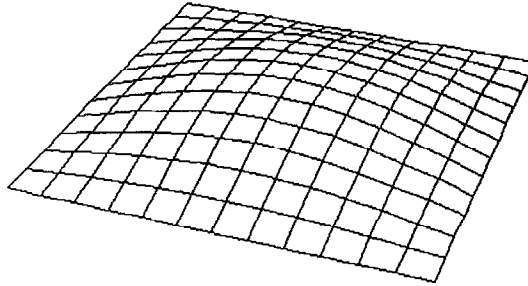


Fig. 12. Buckling load parameter.



(a)



(b)

Fig. 13. Buckling mode and variation of σ_x (at $x = a/2$) as $a/b = 1$: (a) in z - x plane at $y = b/2$; (b) in 3-D form.

where

$$(\delta N_x, \delta N_y, \delta N_{xy}, \delta M_x, \delta M_y, \delta M_{xy})$$

$$= \int_{-h/2}^{h/2} (\delta \sigma_x, \delta \sigma_y, \delta \tau_{xy}, z \delta \sigma_x, z \delta \sigma_y, z \delta \tau_{xy}) dz. \tag{8}$$

$$\delta \epsilon_x^0 = \frac{\partial \delta v}{\partial y} + \frac{1}{2} \left(\frac{\partial \delta w}{\partial y} \right)^2 + \frac{\partial w}{\partial y} \frac{\partial \delta w}{\partial y},$$

$$\delta \gamma_{xy}^0 = \frac{\partial \delta u}{\partial y} + \frac{\partial \delta v}{\partial x} + \frac{\partial \delta w}{\partial x} \frac{\partial w}{\partial y} + \frac{\partial w}{\partial x} \frac{\partial \delta w}{\partial y} + \frac{\partial \delta w}{\partial x} \frac{\partial w}{\partial y}, \tag{10}$$

The relations between the incremental strains and displacements are

$$\begin{cases} \delta \epsilon_x = \delta \epsilon_x^0 + z \delta k_x, \\ \delta \epsilon_y = \delta \epsilon_y^0 + z \delta k_y, \\ \delta \gamma_{xy} = \delta \gamma_{xy}^0 + z \delta k_{xy}, \end{cases} \tag{9}$$

$$\delta k_x = -\frac{\partial^2 \delta w}{\partial x^2},$$

$$\delta k_y = -\frac{\partial^2 \delta w}{\partial y^2},$$

$$\delta k_{xy} = \frac{\partial^2 \delta w}{\partial x \partial y}.$$

where

$$\delta \epsilon_x^0 = \frac{\partial \delta u}{\partial x} + \frac{1}{2} \left(\frac{\partial \delta w}{\partial x} \right)^2 + \frac{\partial w}{\partial x} \frac{\partial \delta w}{\partial x},$$

The results of the present study are compared with those of Harik and Ekambarom [9] in Fig. 12, which demonstrates the applicability and reliability of the

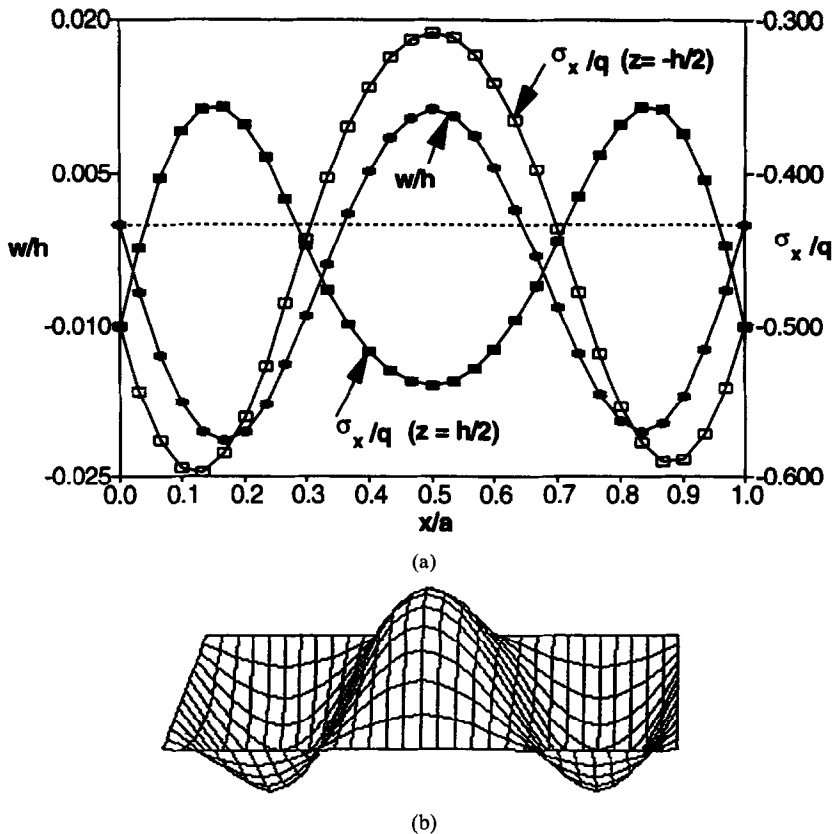


Fig. 14. Buckling mode and variation of σ_x (at $x = a/2$) as $a/b = 3$: (a) in z - x plane at $y = b/2$; (b) in 3-D form.

proposed algorithm for analysing structural problems. The predicted buckling modes for two different ratios of the edge lengths of the plate i.e. $a/b = 1$ and 3, are presented in Figs 13 and 14. The buckling mode is only one wave when $a/b = 1$, but becomes three when $a/b = 3$ in the direction of loading. Figures 13(a) and 14(a) also exhibit the variation of normal stress σ_x in the post-buckling stage. Since the plate is subjected to a unidirectional compressive force, all nodes have the same normal stress σ_x in the pre-buckling stage. However, because of the bending effect in the post-buckling deformation, σ_x varies.

4. CONCLUSIONS

The DXDR method has been combined with the dynamic criterion of stability to analyse the elastic wrinkling/buckling and post-wrinkling/buckling of plate components. An algorithm for predicting bifurcation events has been proposed and found to be efficient. The applicability and reliability of the method has been demonstrated through a detailed analysis of a number of practical deformation problems. Some approximate relationships to determine the number of waves and critical loads of annular plates have been presented. The method presented herein can be used to study more

complicated engineering problems associated with wrinkling/buckling and post-wrinkling/buckling.

REFERENCES

1. L. C. Zhang, T. X. Yu and R. Wang, Investigation of sheet metal forming by bending—part II. Plastic wrinkling of circular sheets pressed by cylindrical punches. *Int. J. Mech. Sci.* **321**, 301–308 (1989).
2. L. C. Zhang and T. X. Yu, Modified adaptive dynamic relaxation method and its application to elastic–plastic bending and wrinkling of circular plates. *Comput. Struct.* **33**, 609–614 (1989).
3. N. Yamaki and Sendai, Buckling of a thin annular plate under uniform compression. *ASME, J. Appl. Mech.* **25**, 267–273 (1958).
4. O. Majima and K. Hayashi, Elastic buckling and flexural vibration of annular plates under axisymmetric in-plane forces. *Bull. JSME* **27**, 2088–2094 (1984).
5. T. X. Yu and W. Johnson, The buckling of annular plates in relation to the deep-drawing process. *Int. J. Mech. Sci.* **24**, 175–188 (1982).
6. T. X. Yu and L. C. Zhang, The elastic wrinkling of an annular plate under uniform tension on its inner edge. *Int. J. Mech. Sci.* **28**, 729–737 (1986).
7. T. X. Yu and W. J. Stronge, Wrinkling of a circular elastic plate stamped by a spherical punch. *Int. J. Solids Struct.* **21**, 995–1003 (1985).
8. L. C. Zhang, T. X. Yu and R. Wang, Investigation of sheet metal forming by bending—part IV: bending and wrinkling of circular sheets pressed by a

hemispherical punch. *Int. J. Mech. Sci.* **31**, 335–348 (1989).

9. I. E. Harik and R. Ekambaram, Seminumerical solution for buckling of rectangular plates. *Comput. Struct.* **23**, 649–655 (1986).
10. L. C. Zhang, M. Kadkhodayan and Y-W Mai, Development of maDR method. *Comput. Struct.* **52**, 1–8 (1994).

APPENDIX

The DXDR method

In the DXDR method, the governing equations of a static system,

$$\mathbf{P}(\mathbf{X}) = \mathbf{F}, \tag{A1}$$

is first replaced by its corresponding dynamic ones,

$$\mathbf{M}\ddot{\mathbf{X}} + \mathbf{C}\dot{\mathbf{X}} + \mathbf{P}(\mathbf{X}) = \mathbf{F}, \tag{A2}$$

where \mathbf{P} , \mathbf{X} and \mathbf{F} are the vectors of internal forces, the approximate solution and the external forces of discrete system, respectively. The mass and damping matrices, \mathbf{M} and \mathbf{C} , are fictitiously chosen as diagonal ones so that the static solution could be obtained in minimum number of pseudo-time steps. All the calculations become explicit when the central finite difference scheme is used. The explicit formulation for the solution vector \mathbf{X} is given by,

$$\dot{\mathbf{x}}_i^{n+1/2} = \frac{2 - \tau^n \zeta_i^n}{2 + \tau^n \zeta_i^n} \dot{\mathbf{x}}_i^{n-1/2} + \frac{2\tau^n}{2 + \tau^n \zeta_i^n} (\mathbf{m}_i^n)^{-1} \mathbf{R}_i^n, \tag{A3}$$

$$\mathbf{x}_i^{n+1} = \mathbf{x}_i^n + \tau^{n+1} \dot{\mathbf{x}}_i^{n+1/2}, \quad (i = 1, \dots, N_{\text{total}}) \tag{A4}$$

where τ^n is the pseudo-time increment of the n th iteration and $\mathbf{R}^n = \mathbf{F} - \mathbf{P}(\mathbf{X}^n)$ is the disequilibrium internal forces. ζ_i^n is the node damping factor at the n th iteration and is calculated by

$$\zeta_i^n = 2 \left(\frac{(\mathbf{x}_i^n)^T \mathbf{P}_i^n}{(\mathbf{x}_i^n)^T \mathbf{m}_i^n \mathbf{x}_i^n} \right)^{1/2}. \tag{A5}$$

The initial $\bar{\mathbf{X}}^0$ for iteration is determined by

$$\bar{\mathbf{X}}^0 = \frac{1}{2}(\mathbf{X}^0 + \mathbf{X}^*), \tag{A6}$$

where \mathbf{X}^0 and \mathbf{X}^* indicate, respectively, the initially guessed solution and the peaks of locus of \mathbf{X} during iteration without damping. The elements of \mathbf{M} are determined by the Gerschgorin theorem, i.e.

$$m_{ii}^L \geq \frac{1}{4}(\tau^n)^2 \sum_j |k_{ij}|, \quad (L = u, v, w) \tag{A7}$$

where m_{ii}^L is the fictitious mass in direction L on node i (whereas \mathbf{m}_i in eqn (A5) is the fictitious sub-mass matrix for each node), and k_{ij} is the element of the stiffness matrix of the system, \mathbf{K} , determined by

$$\mathbf{K} = \frac{\partial \mathbf{P}(\mathbf{X})}{\partial \mathbf{X}}. \tag{A8}$$

More detailed discussions and descriptions can be found in [10].